UCLA
UCLA Previously Published Works

Title

Evolution of Coagulation-Fragmentation Stochastic Processes Using Accurate Chemical Master Equation Approach.

Permalink

https://escholarship.org/uc/item/6w5663nr

Journal

Communications in Information and Systems, 19(1)

Authors

Manuchehrfar, Farid
Tian, Wei
Chou, Tom
et al.

Publication Date

2019

DOI

10.4310/cis.2019.v19.n1.a3

Peer reviewed

eScholarship.org Powered by the California Digital Library
University of California

Author Manuscript

Author Manuscript

Author Manuscript

Author Manuscript

HHS Public Access

Author manuscript

Commun Inf Syst. Author manuscript; available in PMC 2021 August 20.

Published in final edited form as:

Commun Inf Syst. 2019 ; 19(1): 37–55. doi:10.4310/cis.2019.v19.n1.a3.

Evolution of Coagulation-Fragmentation Stochastic Processes Using Accurate Chemical Master Equation Approach

Farid Manuchehrfar[*], **Wei Tian**[*], **Tom Chou**[†], **Jie Liang**[*,‡]

[*]Department of Bioengineering, University of Illinois at Chicago (UIC), Chicago, Illinois, USA.

[†]Departments of Biomathematics and Mathematics, University of California at Los Angeles (UCLA), Los Angeles, California

Abstract

Coagulation and fragmentation (CF) is a fundamental process in which smaller particles attach to each other to form larger clusters while existing clusters break up into smaller particles . It is a ubiquitous process that plays important roles in many physical and biological phenomena. CF is typically a stochastic process that often occurs in confined spaces with a limited number of available particles . Here, we study the CF process formulated with the discrete Chemical Master Equation (dCME). Using the newly developed Accurate Chemical Master Equation (ACME) method, we examine the time-dependent behavior of the CF system. We investigate the effects of a number of important factors that influence the overall behavior of the system, including the dimensionality, the ratio of attachment to detachment rates among clusters, and the initial conditions. By comparing CF in one and three dimensions, we conclude that systems in three dimensions are more likely to form large clusters. We also demonstrate how the ratio of the attachment to detachment rates affects the dynamics and the steady-state of the system. Finally, we demonstrate the relationship between the formation of large clusters and the initial condition.

1 Introduction

Coagulation and fragmentation (CF) is a fundamental process in which particles attach to each other to form larger clusters which can also break down into smaller ones. The general mechanism presents itself in physical processes such as spray and aerosol [1, 2, 3], biological processes such as filament formation and capsid protein nucleation [4, 5], and biomedical phenomena such as blood clotting [6, 7, 8, 9, 10].

The CF problem has been the focus of numerous theoretical and experimental studies [12, 13, 7, 11]. Smolukowski's equation and the mass-action based Becker-Döring (BD) equation have been the basis of many studies [19, 20, 21, 13]. Solving these equations usually requires an assumption of infinite system size. However, CF often occurs in confined spaces with limited numbers of molecules [13]. The behavior of CF in such small systems is also intrinsically stochastic and the effects of the discreteness in particle and cluster numbers is significant.

[‡]To whom correspondence should be addressed, Professor. Jie Liang: jliang@uic.edu.

Author Manuscript Author Manuscript Author Manuscript Author Manuscript

In addition, the CF process lies at the heart of the blood clotting phenomenon [14]. The full coagulation cascade involves many molecular species and numerous reactions, often requiring complex models such as the ordinary differential equation (ODE) model of Hockin *et al.* (with 34 species and 42 rates) [15], or an even more complex platlet-plasma model of [16]. However, key steps involving the formation cluster of fibrin particles can be regarded as a CF process [17], similar to the subject of this study.

Hockin-Mann reaction network model and classic Becker-Döring-type models do not incorporate discreteness and stochasticity of the CF process, when it happens in confined space [22, 13]. However, the Chemical Master Equation (CME) approach is widely used to address discreteness and stochasticity [23, 24, 25]. Solving the CME provides an evolving landscape in state space while the discrete form of the CME (dCME) can account for finite size effects [26, 27, 28].

Monte Carlo (MC) simulation is commonly used to solve the discrete CME [29, 30, 31, 32]. Studies based on MC simulations can incorporate both attachment and detachment reactions, discreteness, and stochasticity of the processes. However, they are limited by the efficiency of sampling and only provide trajectories obeying the dCME. To the best of our knowledge, there is no MC-based approach that can easily simulate the CF across all ranges of the attachment and detachment rates, in various dimensions, and with different initial conditions.

An alternative approach is to obtain an exact solution to the dCME. This is made possible only by using the newly developed Accurate Chemical Master Equation (ACME) algorithm [33]. Using ACME, we first enumerate all the microstates reachable by the CF process given a specific initial condition [34]. We then find the transition matrix connecting these microstates which will be used to determine the time-evolution and steady state of the probability distribution of the system. Using this approach, we will analyze how dimensionality of the system, the ratio of attachment to detachment rates among clusters, and initial conditions affect on the CF process.

2 Method

We describe the CF process using the discrete Chemical Master Equation (dCME) [35]. In our CF problem, there exists N molecular species $n_1, n_2, \ldots, n_N$ and m reactions with reaction rate constants $r_1, r_2, \ldots, r_m$. The k-th reaction is represented as

$$c_{1,k}n_1 + c_{2,k}n_2 + \ldots + c_{N,k}n_N \xrightarrow{r_k} c'_{1,k}n_1 + c'_{2,k}n_2 + \ldots + c'_{N,k}n_N \quad (1)$$

We assume the fixed-volume system is well-mixed.

The microstate of the system at time t can be represented with a vector of the copy number of each species: $x(t) = (x_1(t), x_2(t), \ldots, x_N(t)) \in \mathbb{R}^N$. The union of all possible microstates of the system across all times forms the state space of the system S.

The rate of the k-th reaction which causes the transition of the system from microstate j to microstate i is defined as

Author Manuscript Author Manuscript Author Manuscript Author Manuscript

$$A_k(x_i, x_j) \equiv r_k \prod_{z=1}^{N} \binom{x_z}{c_{z,k}} \tag{2}$$

Using the definitions above, the discrete Chemical Master Equation can be written as

$$\frac{\partial p(x,t)}{\partial t} = \sum [A(x,x')p(x',t) - A(x',x)p(x,t)] \tag{3}$$

Here, $p(x, t)$ is the probability of the microstate x, and $A(x, x')$ is the transition rate from microstate x' to microstate x. We can compute the probability $p(x, t)$ from Eq. (3) using the Accurate Chemical Master Equation (ACME) method [33].

In our finite-sized system, we assume there is a source reservoir of particles with a maximum capacity of M. Individual particles in the system can be generated through a reaction that produces clusters of size 1. Clusters of size 1 can also be removed through a degradation reaction, which deposits one particle back into the source. Furthermore, a cluster of size i and a cluster of size j can attach to each other and form a new cluster of size $(i + j)$, while $(i + j)$ cannot exceed a maximum cluster size of N. Clusters of size $(i + j)$ can also degrade into two clusters of size i and j via detachment reaction (see Fig. 1). Thus, we have four reactions of attachment, detachment, synthesis, and degradation (Eq. (4–7)) in our CF system

$$X_i + X_j \xrightarrow{\mathrm{a_{i,j}}} X_{i+j}, \quad A_{att,ij} = \begin{cases} a_{i\,.\,j} \cdot n_i \cdot (n_j - 1)/2, & \text{if } i = j \\ a_{i\,.\,j} \cdot n_i \cdot n_j, & \text{if } i \neq j \end{cases} \tag{4}$$

$$X_{i+j} \xrightarrow{\mathrm{d_{i,j}}} X_i + X_j, \quad A_{det,ij} = d_{i\,.\,j} \cdot n_{i+j} \tag{5}$$

$$\phi \xrightarrow{\mathrm{k_s}} X_1, \quad A_s = k_s \tag{6}$$

$$X_1 \xrightarrow{\mathrm{k_d}} \phi, \quad A_d = k_d \cdot n_1 \tag{7}$$

Here, X_i represents a cluster of size i, ϕ the source of the system, n_i the copy number of clusters of size i, and $a_{i,j}$ and $d_{i,j}$ the attachment and detachment rate constants, respectively. For one-dimensional (1D) systems, the clusters are linear chains of particles and the attachment and detachment of particles occur only at the ends of the cluster. Thus, the attachment and detachment rates are independent of the length of the cluster and will be taken to be constants. However, in two or three dimensions, both the attachment and detachment rates depend on the size of the clusters involved in the reaction. A simple model may be that these rates depend on the perimeter and surface area of the clusters: $a_{i,j}, d_{i,j} \propto (i \cdot j)^{1/2}$ for 2D systems, and $a_{i,j}, d_{i,j} \propto (i \cdot j)^{2/3}$ for 3D systems [20].

Author Manuscript Author Manuscript Author Manuscript Author Manuscript

To illustrate, we give a simple example in which we have the maximum cluster size $N = 3$ and the maximum total mass of the system $M = 4$. We assume that the system starts from the initial condition where there are 4 particles in the source and there is no cluster present in the system. In this simple system, we can have three different types of clusters, those of size 1, 2, and 3, respectively. Thus, each microstate of the system can be indexed with four integers, the first indicating the number of particles in the source; the second, third, and forth integers indicating the number of clusters with size 1, 2, and 3, respectively. Eq. (8–10) are the reactions in this simple system and the state space of the system is illustrated in Fig. 2.

$$\phi \leftrightarrow X_1 \tag{8}$$

$$2X_1 \leftrightarrow X_2 \tag{9}$$

$$X_1 + X_2 \leftrightarrow X_3 \tag{10}$$

We can then find the rate matrix and compute the probability of each microstate (Table 1). From the probability of each microstate, we can then find the expected number and the probability of each cluster (Eq. (11) and (12), respectively)

$$\langle n_i \rangle = \sum_l P_l \cdot n_i \tag{11}$$

$$P_{n_i} = \sum_l P_l(n_i = 0) \tag{12}$$

where l is the microstate index (Table 1), $\langle n_i \rangle$ the expected number, and P_{n_i} the probability of observing a cluster of size i.

In our study, we shall restrict ourselves to a system with total mass $M = 48$ and a maximum possible cluster size $N = 16$, which are much larger than the parameters in previous studies ($M = 32$, $N = 8$) [30]. To describe the CF system, our state space includes $> 700,000$ microstates. For our calculations, we use a machine with a 20-core Xeon E5–2670 CPU of 2.5GHz, with a cache size of 20MB and 128GB Ram. Computing the steady state distribution at a specific ratio of the attachment to detachment rates ($a_{i,j}/d_{i,j}$) takes about 38 minutes. Computing the time-evolving probability distribution takes between 2,729 min and 3,292 min. Table 2 provides details on the computational cost.

3 Results

Our results are organized as follows. We first examine the effect of dimensionality on the formation of the largest cluster in the system. We then study the effect of different attachment/detachment rate ratios on the formation of clusters and their steady-state distributions. Finally, we examine the effect of different initial conditions on CF dynamics.

Author Manuscript Author Manuscript Author Manuscript Author Manuscript

3.1 Effects of Dimensionality

For 1D systems, the attachment rate $a_{i,j}$ and the detachment rate $d_{i,j}$ are independent of the size of clusters. For 2D and 3D systems, we will assume $a_{i,j} \& d_{i,j} \propto (i \cdot j)^{1/2}$ and $a_{i,j} \& d_{i,j} \propto (i \cdot j)^{2/3}$, respectively [20]. Fig. 3 compares probability of the largest clusters at different time when $a_{i,j}/d_{i,j} = 1$ in systems with different dimensionality. There is significant difference between the 1D system and 2D/3D systems. At long times, the probability of forming largest clusters in 3D is approximately twice of that in 1D. Since the difference in the large-cluster formation probabilities is negligible between 2D and 3D systems, we will use the 3D results for the rest of this paper.

3.2 Steady State Distributions

Expected number of clusters.—Fig. 4A–D shows the expected number of clusters of different sizes for four different values of $a_{i,j}/d_{i,j}$: 0.1, 1, 10, and 1000. The inset shows the distribution of clusters of different sizes at the steady state. When $a_{i,j}/d_{i,j} \ll 1$, all clusters are singletons. When $a_{i,j}/d_{i,j}$ increases, larger clusters form. When $a_{i,j}/d_{i,j} \approx 1000$, all clusters are at their maximum allowed size. The expected number of all clusters at different ratios of attachment to detachment rates is shown in Fig.4E.

Probability of forming clusters of different sizes.—The formation of large clusters is an important issue in CF processes. Without loss of generality, we set a critical probability of having the largest cluster (p_{16}) to be 0.3. Fig. 5 shows the steady state probabilities of different clusters with different $a_{i,j}/d_{i,j}$. When $a_{i,j}/d_{i,j} < 3.0$, p_{16} is less than the probability of other clusters ($p_1 - p_{15}$)(Fig.5A). When this ratio is around 3, the probabilities for all clusters are almost equal. Thus, for the assumed threshold, $a_{i,j}/d_{i,j} = 3.0$ is the critical ratio of attachment to detachment rate. Below this value, forming the largest cluster is unlikely.

3.3 Dynamical Behavior of the CF System

The time a CF system needs to reach the critical probability of p_{16} is a quantity of interest. We therefore examine the dynamics of the system to understand the time-dependence of forming large clusters. Fig.6A shows how p_{16} grows for different ratios of attachment to detachment rates. When $a_{i,j}/d_{i,j} < 3$, the probability of forming the largest cluster is less than 0.3, regardless of how much time has past. Fig.6B shows the critical time at which the probability of forming the largest cluster reaches 0.3 (white region). Before this critical time, formation of large clusters is unlikely to occur (blue region). A system containing large clusters are more likely after this critical time (red region). In extreme cases when $a_{i,j}/d_{i,j} > 1000$, it is highly probable that large clusters will form in the system within 40 minutes. In contrast, when $a_{i,j}/d_{i,j} \approx 3.0$, it takes about 150 minutes for the system to form, with appreciable probability > 0.3, a maximum-size cluster (Fig.6B).

We examined the convergence behavior in reaching the steady state distribution. Table. 3 lists the distance to the steady state measured as $|p_{16}(\infty) - p_{16}(t)|$ at different time and with different $a_{i,j}/d_{i,j}$. Larger $a_{i,j}/d_{i,j}$ leads to faster convergence.

Following [5], we analyzed the elasticity and sensitivity of parameters of the CF system for a subset of clusters present at different ratio of $a_{i,\mathrm{J}}/d_{i,\mathrm{J}}$. Here, we use sensitivity to examine

Author Manuscript Author Manuscript Author Manuscript Author Manuscript

the response of the expected number of different clusters to changes in $a_{i,J}/d_{i,J}$. We use elasticity to examine the relative changes in the expected number of different clusters with respect to the relative changes in $a_{i,J}/d_{i,J}$. Following [5], the sensitivity Se and the elasticity El of forming a cluster of size i are calculated as

$$Se = \frac{\partial \langle n_i \rangle}{\partial \left(a_{i,\,j}/d_{i,\,j} \right)} \tag{13}$$

$$El = \frac{\frac{\partial \langle n_i \rangle}{\langle n_i \rangle}}{\frac{\partial \left(a_{i,\,j}/d_{i,\,j} \right)}{\left(a_{i,\,j}/d_{i,\,j} \right.}} = \frac{\left(a_{i,\,j}/d_{i,\,j} \right)}{\langle n_i \rangle} \cdot Se \tag{14}$$

Fig. 7 shows Se and El for formation of 4 clusters of sizes 4, 8, 12, and 16 at 3 different $a_{i,J}/d_{i,J}$ of 5, 20, and 50. When $a_{i,J}/d_{i,J}$ increases, Se and El decreases for forming clusters of different sizes. In addition, we found that smaller clusters have higher Se and El.

3.4 Dependence on Initial Conditions

In the examples above, we assumed 48 particles are initially in the source which can be transported into the system through synthesis reactions. We now examine the effect of different initial conditions on the formation of the maximum-sized clusters and the time it takes for the system to approach steady state.

We start with different initial conditions constrained to having the same initial mean size (IMS) of clusters. Fig. 8 shows the evolutions of the probability of formation of the largest cluster for four different initial conditions: 12 clusters of size 4 ($12 \cdot n_4$), 6 clusters of size 3 and 6 clusters of size 5 ($6 \cdot n_3 + 6 \cdot n_5$), 6 clusters of size 2 and 6 clusters of size 6 ($6 \cdot n_2 + 6 \cdot n_6$), 6 monomers and 6 clusters of size 7 ($6 \cdot n_1 + 6 \cdot n_7$). All these initial conditions have the same mean cluster size of 4. When the IMSs are the same, systems with different initial conditions show very similar dynamics. Fig.8 shows the behavior of the system in formation of local clusters when the initial conditions have same mean size of clusters.

For systems with different IMSs, the dynamics on the “distance” of the IMS from the steady state mean cluster size distribution (shown in Fig.4E). Figs.9A–B show the time-dependent behavior of the probability of forming the largest cluster under initial conditions with different IMSs and $a_{i,j}/d_{i,j} = 3.0$ and $a_{i,j}/d_{i,j} = 5.0$, respectively. When $a_{i,j}/d_{i,j} = 3.0$ and 5, the mean size of clusters at the steady state is about 8 and 9, respectively (Fig.4E). Figs. 9A–B show the time required for the system to approach steady state for different IMSs. Not surprisingly, the time to approach the steady-state distribution for values of IMS that are closer to the steady-state mean cluster sizes is less.

Figs.9C–D show the time required for the system to reach the steady state for $a_{i,j}/d_{i,j} = 3.0$ and $a_{i,j}/d_{i,j} = 5.0$, respectively. Our results show that the closer the mean size of clusters at the initial condition is to that of the steady state, the less time it takes for the system to approach the stationary distribution. However, we observe that, qualitatively, systems started

Author Manuscript Author Manuscript Author Manuscript Author Manuscript

at IMSs greater than the mean sizes at steady state take longer to relax than those started at IMSs smaller than that at steady state.

When the IMS is larger than the steady state mean size of clusters, larger detachment rates are required for the system to reach the steady state rapidly. However, we have $a_{i,j}/d_{i,j} > 1$. Thus, we observe asymmetry on different side of the steady state (Fig.9C and D). The asymmetry becomes even larger when $a_{i,j}/d_{i,j}$ increases. As a result, the time required for reaching the steady state increases dramatically when IMS become more than the steady state mean size of clusters.

4 Summary and Conclusions

The coagulation and fragmentation is a fundamental mechanism that plays a critical role in many physical and biological processes. Here we studied the general properties of the CF process using the Accurate Chemical Master Equation (ACME) method [33], which can provide accurate solutions to the discrete Chemical Master Equation (dCME) and can account for the stochasticity and the discreteness of the CF process.

We examined how the dimensionality of the clusters affects its behaviors given the same intrinsic attachment and detachment rates. Three-dimensional systems exhibit faster dynamics compared to systems in 1D or 2D. The dimensionality of the clusters affects the effective rates of attachment and detachment, which will determine the speed of particle attachmment and detachment in a cluster.

Steady-state probability distributions of cluster sizes were also studied under varying attachment/detachment rate ratios. For a given critical probability of emergence of maximum-sized clusters, we are able to determine the critical ratio between the attachment and detachment rates. Below this critical ratio, the large cluster of interest is unlikely to form regardless of time. For systems with ratio larger than the critical one, we are able to calculate the time required for the system to form maximum-sized cluster with high probability [36, 37].

We further studied how different initial conditions affect the behavior of the system and find the initial mean size of the clusters is one of the most important factors that govern CF dynamics. We find that the dynamics of systems started with different initial configurations with the same initial mean cluster sizes are similar. Further investigation shows that the dynamics towards steady state are controlled by the deviation of the mean initial cluster size from the mean cluster size at steady state.

Future studies include analysis of various processes of self-assemblies of different molecular and mesoscopic-particles that occur in small closed systems, with supply of limited number of particles. Systems with different binding mode and binding geometry can be explored in details. An example is the HIV-1 viral capsid nucleation process [5]. In addition, critical steps of the blood-clotting processes involving fibrin and other molecules in the blood-clotting process [17] can also be studied.

Author Manuscript Author Manuscript Author Manuscript Author Manuscript

Acknowledgments

JL acknowledges support from the National Institute of Health (R35GM127084, R01CA204962-01A1, and R21 AI126308). TC acknowledges support from the Army Research Office (W911NF-18-1-0345) and the National Science Foundation (DMS-1516675 and DMS-1814364).

References

[1]. Tsantilis S and Pratsinis E Evolution of Primary and Aggregate Particle-Size Distributions by Coagulation and Sintering. Aiche Journal, 46(2):407–415, 2000.

[2]. Goudeli Erini, Eggersdoref Maximilian L. and Pratsinis Sotiris E. CoagulationAgglomeration of Fractal-like Particles: Structure and Self-Preserving Size Distribution. Langmuir, 31(4):1320–1327, 2015. [PubMed: 25560979]

[3]. Hadi Keramati, Saidi Mohammad Hassan and Mohammad Zabetian Stabilization of the Suspension of Zirconia Microparticle Using the Nanoparticle Halos Mechanism: Zeta Potential Effect. Journal of Dispersion Science and Technology, 37(1):6–13, 2016.

[4]. Sept David and McCammon JA Thermodynamics and kinetics of actin filament nucleation. Biophysical Journal, 81(2):667–674, 2001. [PubMed: 11463615]

[5]. Sadre-Marandi Farrah, Liu Yuewu, Liu Jiangguo, Tavener Simon, Zou XiufenModeling HIV-1 viral capsid nucleation by dynamic systems. Mathematical Biosciences, 270:95–105, 2015. [PubMed: 26596714]

[6]. Powers ET and Powers DL The Kinetics of Nucleated Polymerizations at High Concentration: Amyloid Fibril Formation Near and Above the Super Critical Concentration. Biophysical Journal, 91:122–132, 2006. [PubMed: 16603497]

[7]. Edelstein-Keshet Leah and Ermentrout G. Bard Models for the length distributions of actin filaments: I. Simple polymerization and fragmentation. Bulletin of Methematical Biology, 60, 1998.

[8]. Nurden Alan TThe biology of the platelet with special reference to inflammation, wound healing and immunity. Frontiers in Bioscience, 23:726–751, 2018.

[9]. Bertsch Michiel, Franchi Bruno, Marcello Norina, Tesi Maria Carla, Tosin AndreaAlzheimers Disease: a Mathematical Model for Onset and Progression, Mathematical Medicine and Biology. Italian Ministary of Health, 34(2):193–214, 2017.

[10]. Tarbox Abigail K. and Swaroop Mamta Pulmonary embolism. International Journal of Critical Illness and Injury Science, 3(1):69–72, 2013. [PubMed: 23724389]

[11]. Krapivsky Pavel L. and Redner Sidney and Ben-Naim Eli A Kinetic View of Statistical Physics. Cambridge University Press, Cambridge, UK, 2010.

[12]. Ziff RM and Stell G Kinetics of Polymer Gelation. The Journal of Chemical Physics, 73(7):3792, 1980.

[13]. Wattis Jonathan A. D. and King John R. Asymptotic solutions of the Becker-Dring. Journal of Physics A: Mathematical General, 31:7169–9189, 1998.

[14]. Englemann BerndInitiation of coagulation by tissue factor carriers in blood. Blood Cells, Molecules, and Diseases , 36:188–190, 2006.

[15]. Hockin Matthew F., Jones Keneth C., Everse Stephen J., Mann Kenneth G.A model for the stoichiometric regulation of blood coagulation. The Journal of Biological Chemistry, 227(21):18322–18333, 2002.

[16]. Chatterjee Manash S., Denney William S., Jing Huiyan, Diamond Scott L.System biology of coagulation initialtion: Kinetics of thrombin generation in resting and activated human blood. PLOS Computational Biology, 6(9):e1000950, 2010. [PubMed: 20941387]

[17]. Guy Robert D., Fogelson Aaron L., Keener James P.Fibrin gel formation in a shear flow. Mathematical Medicine and Biology, 0:1–20, 2005.

[18]. Mounts William M., Liebman Michael N.Qualitative modeling of normal blood coagulation and its pathological states using stochastic activity networks. International Journal of Biological Macromolecules, 20:265–281, 1997. [PubMed: 9253647]

Author Manuscript Author Manuscript Author Manuscript Author Manuscript

[19]. Hoze Nathanael and Holcman David Stochastic coagulation-fragmentation processes with a finite number of particles and applications. Annals of Applied Probability, 28(3):1449–1490, 2016.

[20]. Niethammer BOn the Evolution of Large Clusters in the Becker-Dring Model. Journal of Nonlinear Science, 13(1):115–155, 2003.

[21]. Penrose O. The Becker-Dring equations at large times and their connection with the LSW theory of coarsening. Journal of Statistical Physics, 89(1–2):305–320, 1997.

[22]. Davis JK and Sindi SS Initial condition of stochastic self-assembly. Physical Review E, 93(2):022109, 2016. [PubMed: 26986290]

[23]. Gupta Ankit, Mikelson Jan and Khammash Mustafa A Finite State Projection Algorithm for the Stationary Solution of the Chemical Master Equation. The Journal of Chemical Physics, 147:154101, 2017. [PubMed: 29055349]

[24]. Sudbrack Vtor, Brunnet Leonardo G., de Almeida Rita M.C, Ferreira Ricardo M., Gamermann DanielMaster Equation for Degree Distribution of a Duplication and Divergence Network. Physica A, 509:588–298, 2015.

[25]. Smadbeck Patrick and Kaznessis Tiannis N. Solution of Chemical Master Equations for Nonlinear Stochastic Reaction Networks. Current Opinion in Chemical Engineering., 5:90–95, 2014. [PubMed: 25215268]

[26]. Cao Youfang and Liang Jie Adaptively Biased Sequential Importance Sampling for Rare Events in Reaction Networks with Comparison to Exact Solution from Finit Buffer dCME Method. The Journal of Chemical Physics, 139(2):025101, 2013. [PubMed: 23862966]

[27]. Terebus Anna, Cao Youfang and Liang Jie Exact Computation of Probability LAndscape of Stochastic Networks of Single Input and Coupled Toggle Switch Modules. IEEE Engineering in Medicine and Biology Society (EMBS), 20145228–5231, 2014.

[28]. Cao Youfang, Terebus Anna and Liang Jie State Space Truncation with Quantified Errors for Accurate Solution to Discrete Chemical Master Equation. Bulletin of Mathematical Biology, 78(4): 617–661, 2016. [PubMed: 27105653]

[29]. DOrsogna Maria R., Lakatos G and Chou Tom Stochastic Self-Assembly of Incommensurate Clusters. The Journal of Chemical Physics, 136:0884110, 2012.

[30]. DOrsogna Maria R., Qi Lei and Chou Tom First Assembly Times and Equilibrium in Stochastic Coagulation-Fragmentation. The Journal of Chemical Physics, 143:014112, 2015. [PubMed: 26156470]

[31]. Kotalczyk G and Kruis FE A Monte Carlo Method for the Simulation of Coagulation and Nucleation Based on Weighted Particles and the Concepts of Stochastic Resolution and Merging. Journal of Computational Physics, 340:276–296, 2017.

[32]. Smith Alastair J., Wells Clive G. and Kraft Markus A New Iterative Scheme for Solving the Discrete Smoluchowski Equation. Journal of Computational Physics, 352:373–387, 2018.

[33]. Cao Youfang, Terebus Anna and Liang Jie Accurate Chemical Master Equation Solution Using Multi- Finite Buffers. SIAM Multiscale Modeling and Simulation, 14(2): 923–963, 2016.

[34]. Cao Youfang and Liang Jie Optimal Enumeration of State Space of Finitely Buffered Stochastic Molecular Networks and Exact Computation of Steady State Landscape Probability. BMC Systems Biology, 2(30):1–13, 2008. [PubMed: 18171472]

[35]. Youfang Cao, Terebus Anna and Liang Jie Chapter 3. Modeling Dtochastic Gene Regulatory Networks Using Direct Solutions of Chemical Master Equation and Rare Event Sampling, Book title: Research in Analysis and Modeling of Gene Regulatory Networks, Ivanov Ivan V., Qian Xiaoning and Pal Ranadip. Advance in Medical Technologies and Clinical Practice (AMTCP), Book Series 2016.

[36]. Chou Tom and D'Orsogna Maria R. *First passage Problems in Biology* in Chapter 13: First-Passage Phenomena and Their Applications, editors Ralf Metzler, Gleb Oshanin, and Sidney Redner, World Scientific, 2014

[37]. Yvinec R and D'Orsogna Maria R. and Chou Tom. First passage times in homogeneous nucleation and self-assembly. The Journal of Chemical Physics, 137: 244107, 2012. [PubMed: 23277928]

Author Manuscript Author Manuscript Author Manuscript Author Manuscript

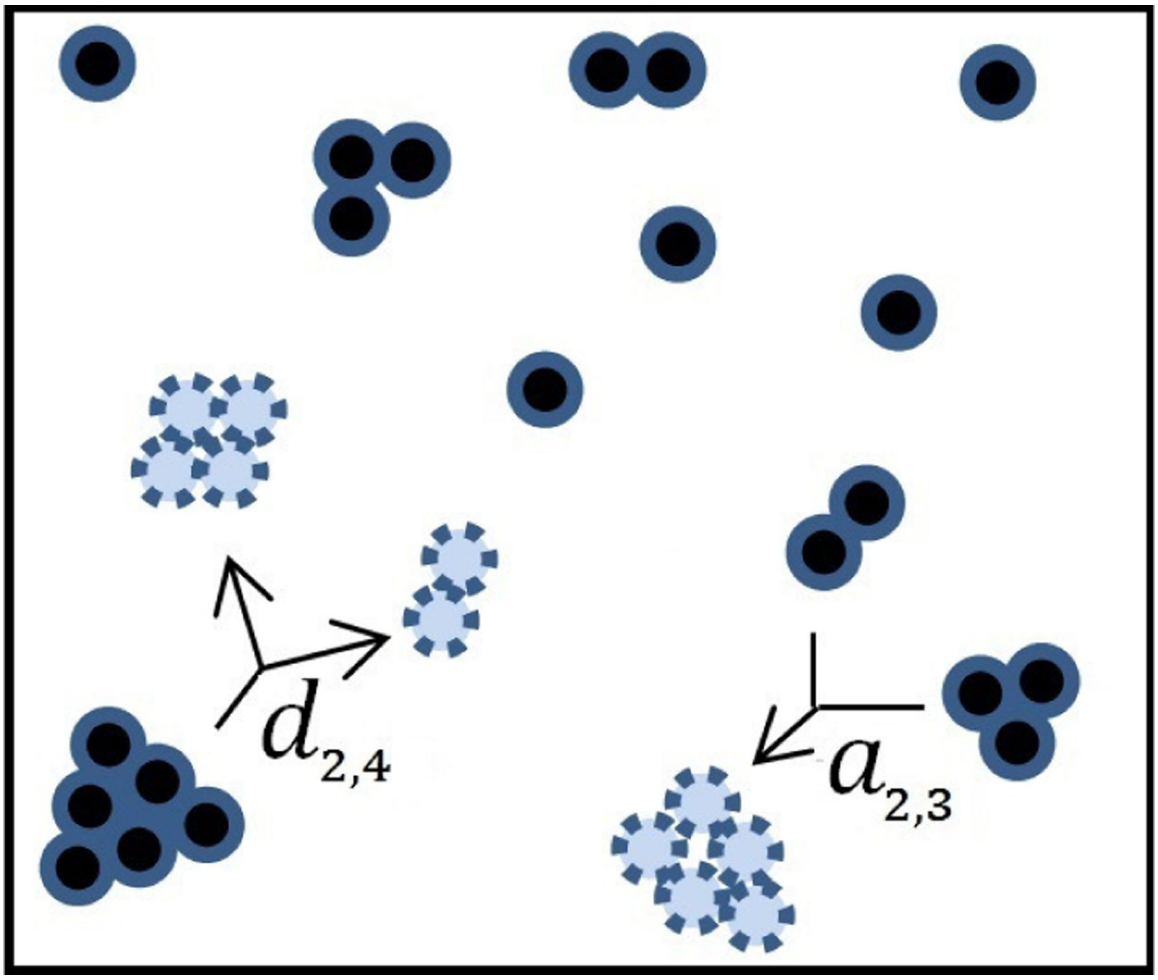

Figure 1:
Schematic of a CF process system showing how particles attach and detach.

Author Manuscript Author Manuscript Author Manuscript Author Manuscript

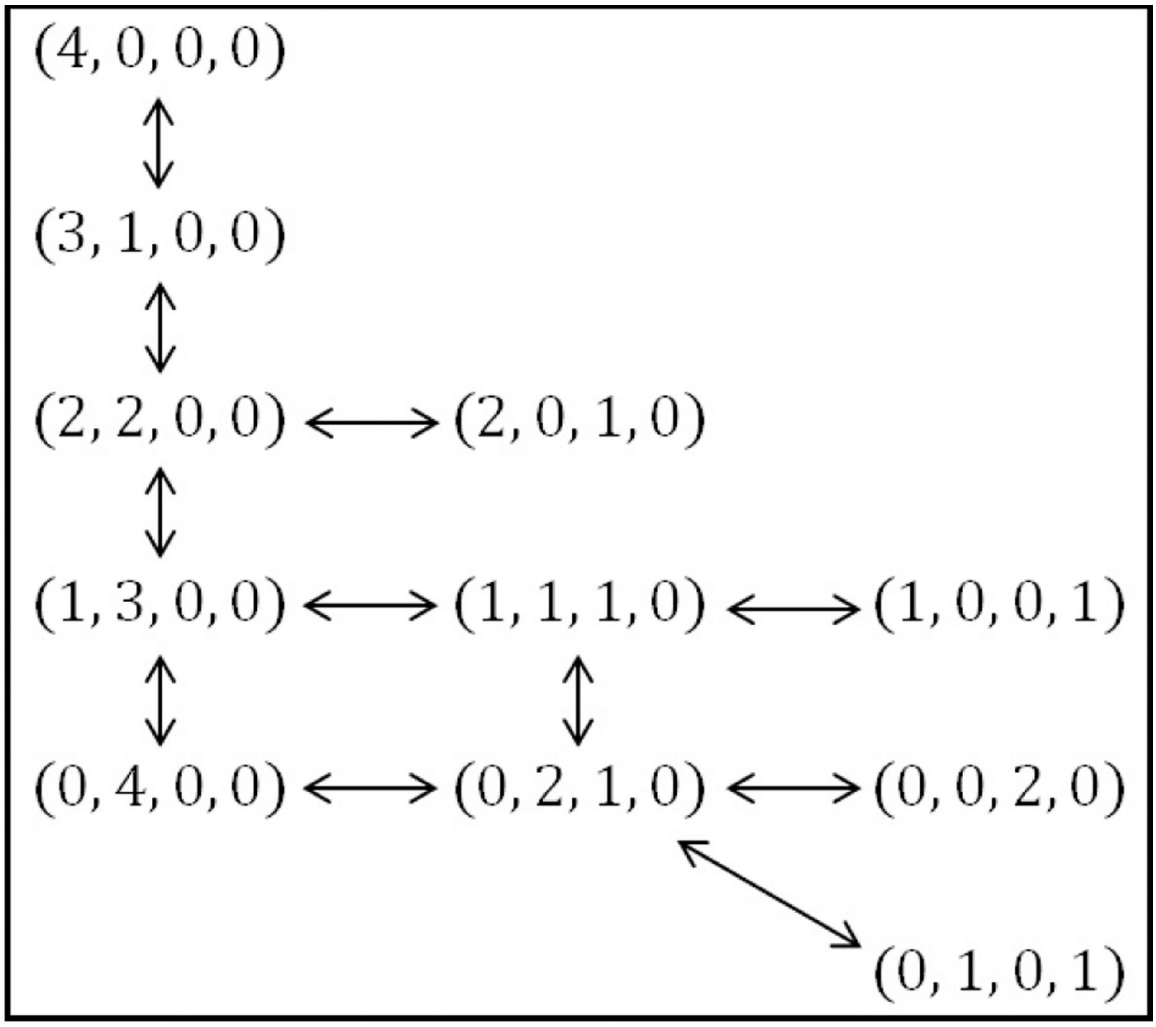

Figure 2:
The state space of a system with a maximum cluster size $N = 3$ and total mass $M = 4$.

Author Manuscript Author Manuscript Author Manuscript Author Manuscript

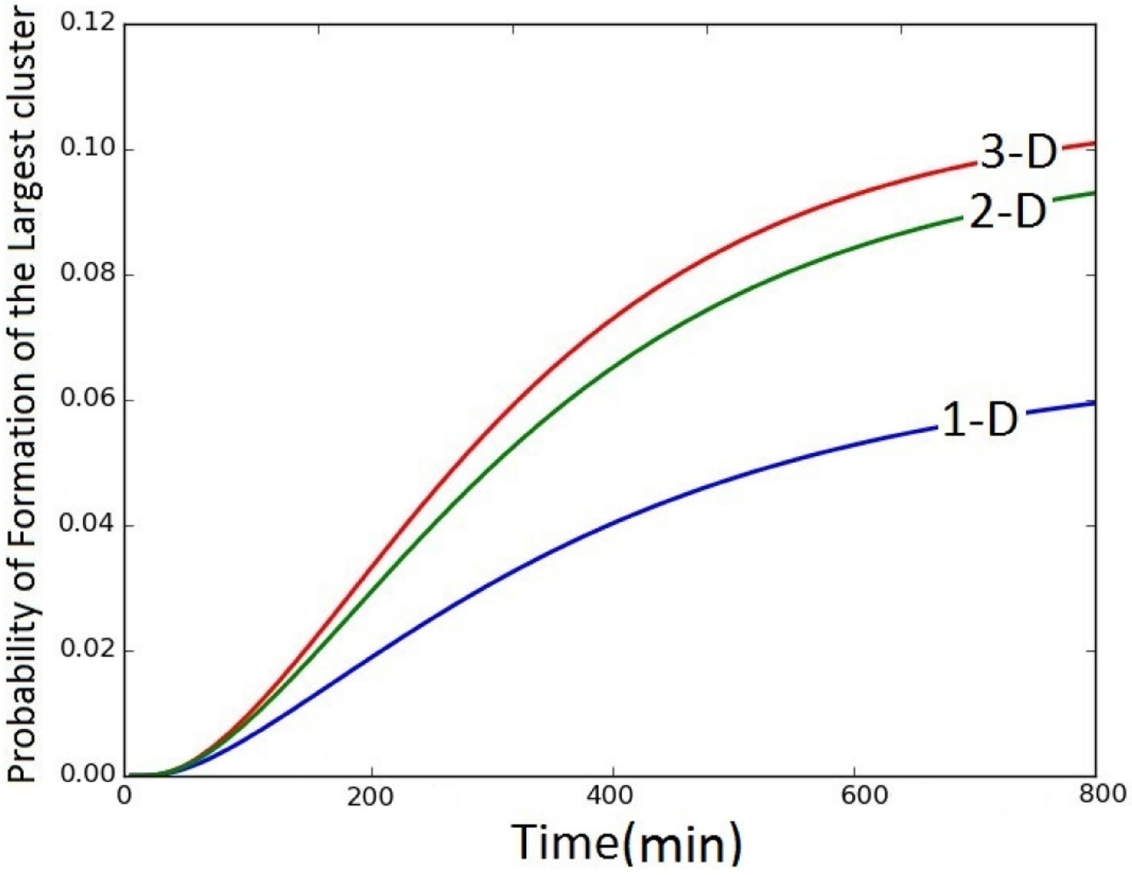

Figure 3:
The probability of formation of the largest cluster at different times in different dimensions when attachment/detachment rates ratio is equal to 1. In 2D/3D systems, this probability is twice of that in 1D while the difference between 2D and 3D systems are negligible.

Author Manuscript Author Manuscript Author Manuscript Author Manuscript

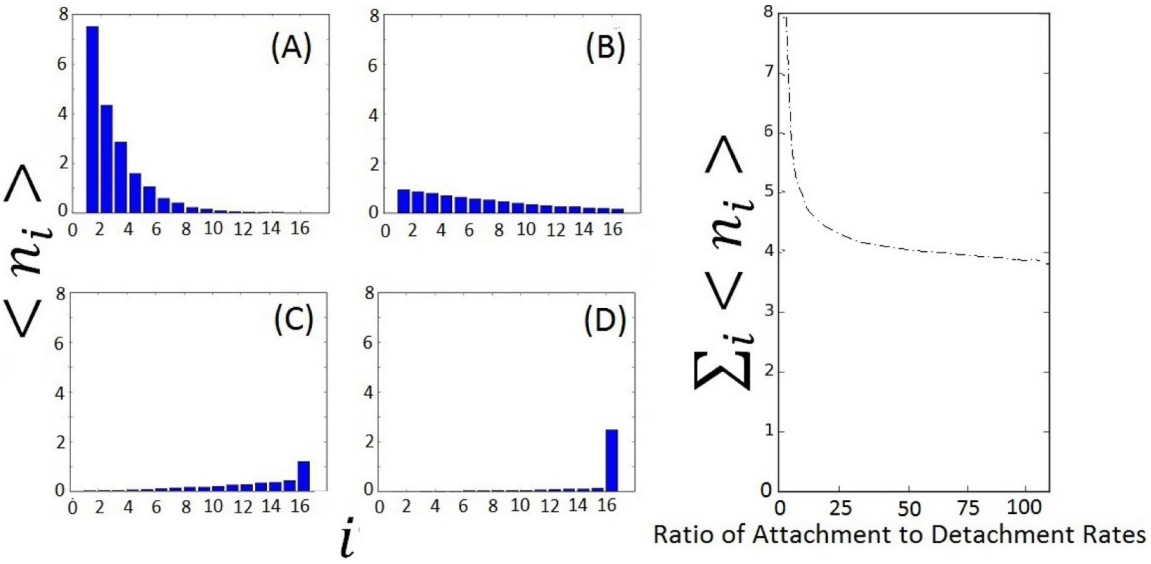

Figure 4:

Expected number of clusters for different $a_{i,j}/d_{i,j}$ at steady state, (A) $a_{i,j}/d_{i,j} = 0.1$, (B) $a_{i,j}/d_{i,j} = 1$, (C) $a_{i,j}/d_{i,j} = 10$, (D) $a_{i,j}/d_{i,j} = 1000$. When $a_{i,j}/d_{i,j}$ increases, expected number of large particles in the system increases. (E) Expected number of clusters of all sizes in the system.

Author Manuscript Author Manuscript Author Manuscript Author Manuscript

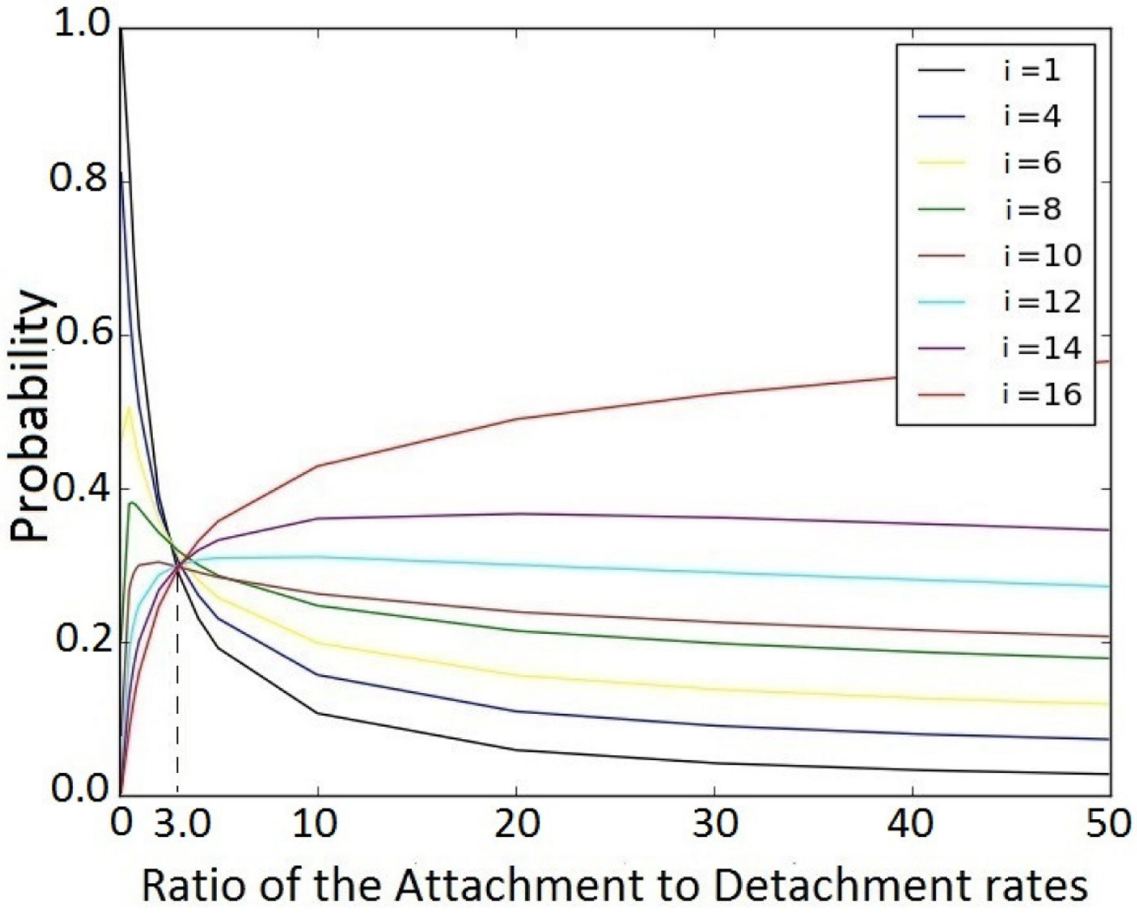

Figure 5:

Probability of local clusters with size i at steady state for different ratios of the attachment to detachment rates.The probability of cluster with size 16 become more than the probability of other clusters when attachment/detachment rate ratio >3 while it is less than the probability of other clusters when attachment/detachment rate ration <3

Author Manuscript Author Manuscript Author Manuscript Author Manuscript

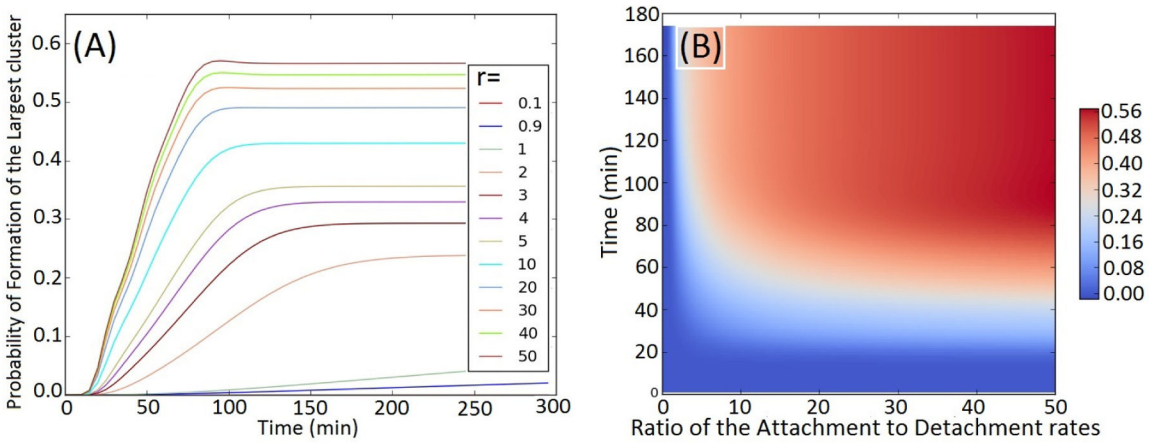

Figure 6:

Time-dependence of the probability to form maximum-size clusters for different ratios r of the attachment to detachment rates. (A): Probability of formation of largest cluster grows when r increases. When $a_{i,j}/d_{i,j} = 3$, probability of formation of largest cluster becomes equal to the critical probability of 0.3, after the system reaches the steady state. (B): Critical time (white region) at which the probability of forming the largest cluster reaches 0.3. Before this critical time (blue region), formation of the largest cluster is unlikely and after this critical time (red region), it is high probable that system contains largest cluster

Author Manuscript Author Manuscript Author Manuscript Author Manuscript

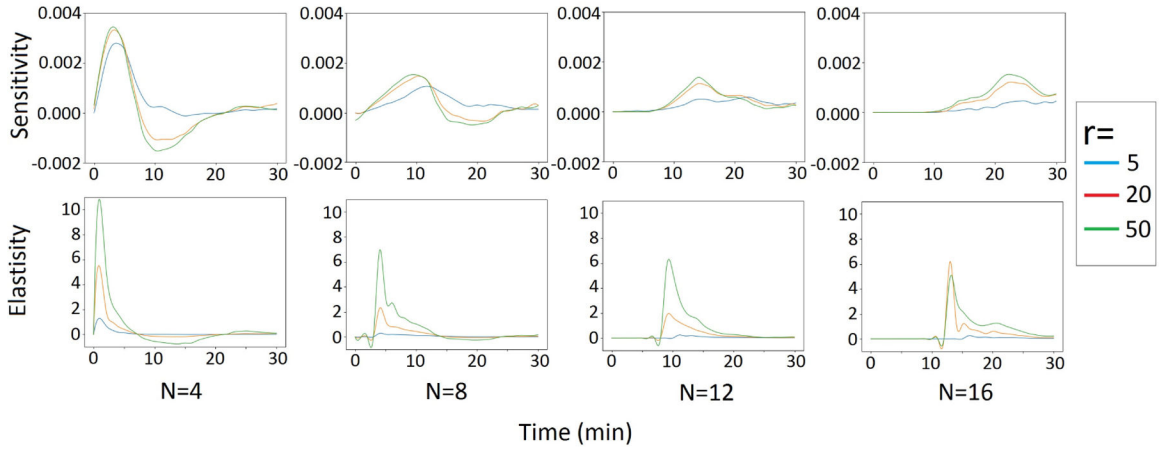

Figure 7:

Sensitivity and elasticity of clusters of size $N = 4, 8, 12, 16$ in response to the ratio r of the attachment to detachment rate $r = 5, 20, 50$: when the size of cluster increase, sensitivity and elasticity of the cluster decrease.

Author Manuscript Author Manuscript Author Manuscript Author Manuscript

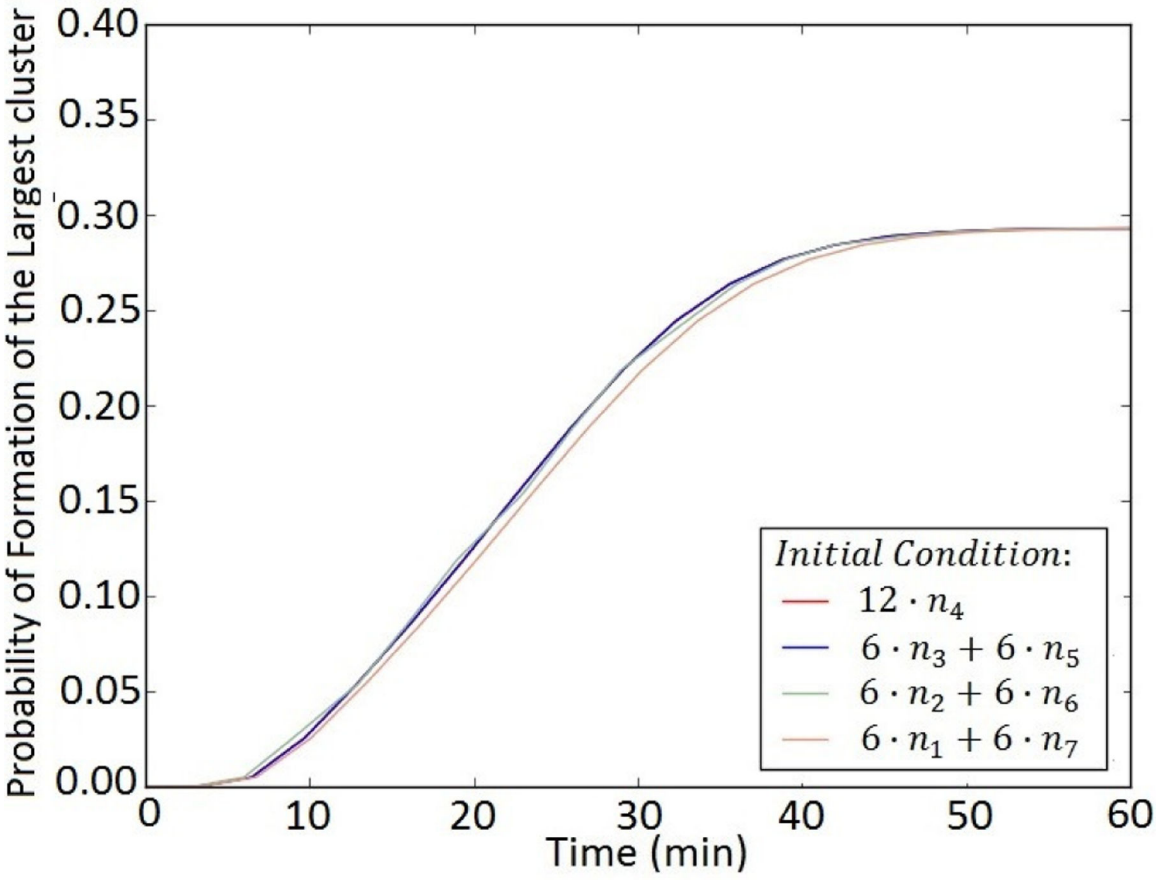

Figure 8:

Probability of formation of largest cluster for different initial conditions where initial conditions have same mean cluster size. When IMSs are the same, different initial conditions show very similar dynamics

Author Manuscript Author Manuscript Author Manuscript Author Manuscript

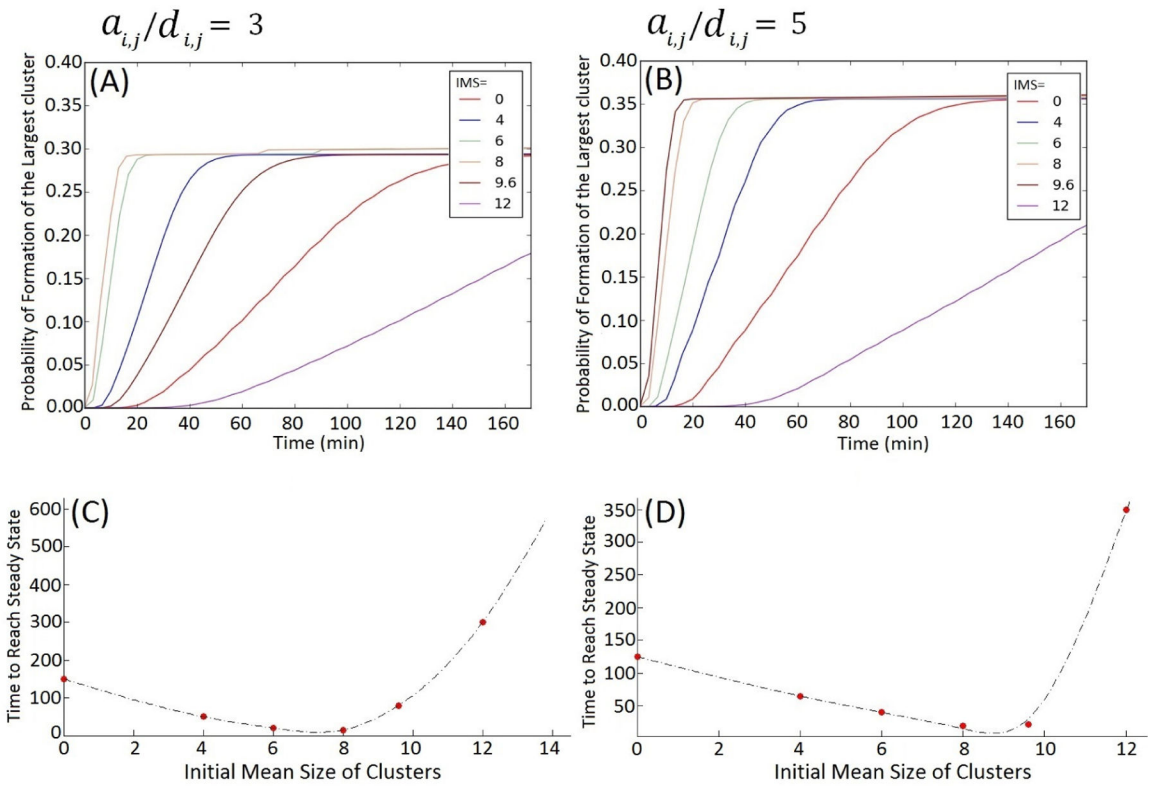

Figure 9:

A–B: Probability of forming maximum-sized clusters for different initial conditions with different initial mean size of clusters at $a_{i,j}/d_{i,j} = 3$ and $a_{i,j}/d_{i,j} = 5$, respectively; C–D: Time that requires for CF system to reach steady state at for different initial conditions at $a_{i,j}/d_{i,j} = 3$ and $a_{i,j}/d_{i,j} = 5$, respectively.

Author Manuscript

Author Manuscript

Author Manuscript

Author Manuscript

Table 1:

Probability of each micro state for our sample example

State index (i)	Prob. (ACME Results)	State (Source, n_1, n_2, n_3)
1	$P_1 = 1.97 \times 10^{-1}$	(4,0,0,0)
2	$P_2 = 1.97 \times 10^{-1}$	(3,1,0,0)
3	$P_3 = 9.84 \times 10^{-2}$	(2,2,0,0)
4	$P_4 = 3.28 \times 10^{-2}$	(2,0,1,0)
5	$P_5 = 8.20 \times 10^{-3}$	(1,3,0,0)
6	$P_6 = 4.92 \times 10^{-2}$	(1,1,1,0)
7	$P_7 = 9.84 \times 10^{-2}$	(1,0,0,1)
8	$P_8 = 9.84 \times 10^{-2}$	(0,4,0,0)
9	$P_9 = 9.84 \times 10^{-2}$	(0,2,1,0)
10	$P_{10} = 9.84 \times 10^{-2}$	(0,0,2,0)
11	$P_{11} = 2.46 \times 10^{-2}$	(0,1,0,1)

Author Manuscript

Author Manuscript

Author Manuscript

Author Manuscript

Table 2:

Computational cost for solving the steady state and the time-evolving dynamics of the system

a_{ij}/d_{ij}	Steady state cost (min)	Time-evolving cost (min)
3.0	38	3, 474
4.0	38	3, 292
5.0	38	3, 152
10.0	38	3, 044
20.0	38	2, 913
30.0	38	2, 808
40.0	38	2, 756
50.0	38	2, 729

Author Manuscript

Author Manuscript

Author Manuscript

Author Manuscript

Table 3:

The convergence behavior of the system at different time steps at different ratios of the attachment to detachment rates

$a_{i,j}/d_{i,j}$	$\lvert p_{16}(\infty)-p_{16}(t)\rvert$							$p_{16}(\infty)$
	t=20	t=40	t=60	t=80	t=100	t=120	t=140	
2.0	0.244	0.229	0.196	0.160	0.121	0.084	0.050	0.248
3.0	0.292	0.254	0.196	0.135	0.075	0.035	0.012	0.298
4.0	0.321	0.262	0.185	0.110	0.047	0.014	0.000	0.331
5.0	0.343	0.266	0.183	0.095	0.035	0.010	0.000	0.358
10.0	0.402	0.277	0.158	0.056	0.008	0.000	0.000	0.429
20.0	0.453	0.296	0.140	0.034	0.000	0.000	0.000	0.492
30.0	0.115	0.306	0.135	0.023	0.000	0.000	0.000	0.525
40.0	0.125	0.318	0.130	0.019	0.000	0.000	0.000	0.550
50.0	0.136	0.327	0.140	0.019	0.000	0.000	0.000	0.571